# Cellular dislocation patterning during plastic deformation

Botond Bakó* and Wolfgang Hoffelner
*Paul Scherrer Institute, 5232 Villigen-PSI, Switzerland*
(Received 10 July 2007; revised manuscript received 27 September 2007; published 13 December 2007)

A simulation of dislocation patterning in a two-dimensional multislip configuration is carried out by means of coarse graining in the presence of plastic strain. In order to study the influence of climb on the dislocation cell pattern formation, fatigue simulations with and without climb mobility are performed and compared. The main result is that, in the presence of climb, cellular structures with well-defined characteristic length emerge, in contrast to the self-similar dislocation patterns developing under similar deformation conditions in the absence of climb. Despite the simplicity of our model, the fractal dimension of the self-similar dislocation patterns emerging without climb confirms the previous results for fcc crystals deformed in a multislip configuration. The cell structures emerging when climb is not negligible (in our simulations a climb mobility 1000 times smaller than the glide mobility was considered) resemble the dislocation patterns seen in thermal recovery or melt-grown experiments.

DOI: 10.1103/PhysRevB.76.214108 PACS number(s): 64.70.Pf, 61.20.Lc, 61.72.Bb, 61.72.Lk

## I. INTRODUCTION

The mechanical properties of nickel-based superalloys, which are candidate materials for heat exchangers, turbine blades, or gas-cooled reactors (currently studied in the Generation IV program[1]), operating at high temperatures under extreme loading conditions, may degrade with time. The general degradation mechanisms of materials include time-dependent deformation, microstructural and compositional changes, corrosion enhanced by the accelerating effects of elevated temperatures, etc. High-speed rotating components are susceptible to component failure due to bearing wear and vibration, failure due to low cycle fatigue (the fatigue of rotating components brought on by the continuous imposing and relaxing of centrifugal force caused by fluctuation in speed or by thermally induced strains), flaws in the material (impurities or voids), etc. Investigation of the dynamic behavior of dislocations, the carriers of plastic deformation, attracts growing interest because of its importance for understanding many properties of plastically deformed crystalline materials. Depending on the materials and the deformation conditions, many different dislocation structures can develop. It is well known that a very heterogeneous dislocation distribution called persistent slip bands in a surrounding "matrix" may form upon cyclic deformation of single crystals. In early transmission electron microscopy (TEM) studies, it was observed that cell structures form at small strains in multislip conditions.[2] Depending on the material parameters and deformation conditions, different types of dislocation patterns are observed also in heavily deformed metals, such as, e.g., cell structures or scale-invariant dislocation patterns.[3] Dislocation patterns appear not only in crystals, but in many other systems, such as, e.g. Wigner crystals,[4] vortex (Abrikosov) lattices,[5] magnetic bubble structures,[6] charge density waves,[7] colloidal lattices,[8] dusty plasma,[9] etc. They determine properties of superconducting films[10] and play a crucial role in melting.[11]

The long-range dislocation-dislocation interactions dominate the plastic current and the motion of dislocations, making the development of a theory of the deformation hard and intractable analytically. As deformation proceeds, the formation of partially ordered dislocation cell structures delineated by a vague three-dimensional (3D) network of dislocation walls can be observed. This ordering also has a strong influence on the tensile and creep strength of the superalloys. Other plastic properties of crystalline materials are also closely related to the dislocation patterning and dynamic properties of dislocation motion. To better understand, to model these properties, and to describe these self-organized structures and dislocation patterns observed by transmission electron microscopy during the past decades, several analytical and computational methods have been developed,[12–30] but we are still far from a complete understanding of these phenomena.

One still open question related to cell and fractal dislocation structures is to explain why in the same material in some conditions the observed dislocation pattern is a scale-invariant structure, and in other TEM micrographs cell structures with a well-defined characteristic length scale are seen. Many authors have proposed that the transition to the cell structure should be considered a noise-generated process.[31–34] Computer simulations also show that for crystals in single-slip configuration the matrix structure can be reproduced[35] and to obtain fractal dislocation structures activation of multiple-slip systems is necessary. Fractal dislocation structures in two-slip configuration were reproduced by two-dimensional (2D) stochastic discrete dislocation dynamics simulations of a fatigued fcc single crystal,[36] but the cell structure was observed only during simulation of a thermal recovery process.[37] The important effect of cross slip was emphasized by Madec *et al.* in Ref. 38. Their 3D dislocation dynamics simulations of multiple slip in fcc crystals can also lead to the formation of cell structures—however, presently it is not possible, due to lack of computing power, to check how they evolve and to check self-similarity properties in the developed microstructures.

The present work is concerned with the modeling of dislocation patterning in multislip systems and a qualitative characterization of the observed cellular dislocation structures.[39] The influence of dislocation climb during fatigue on the pattern formation is explored in the simplest

 

possible multislip model, where a system of straight parallel edge dislocations is considered. In the first part of the paper, we reconsider the continuum dislocation dynamics method based on a coarse-graining technique. In the second part, simulation results on our oversimplified model are presented.

## II. COARSE-GRAINED DISLOCATION DYNAMICS

### A. Field theory of dislocations

Due to the long-range nature of interaction forces the internal force acting on a reference dislocation is the sum of forces created by all the other dislocations of the system. The force from dislocation $B$ acting on dislocation $A$ is given by the Peach-Koehler equation

$$\mathbf{F}^{B,A} = (\mathbf{b}^A \sigma^B) \times \boldsymbol{l}^A, \tag{1}$$

where $\mathbf{b}^A$ is the Burgers vector and $\boldsymbol{l}^A$ represents the sense vector of dislocation $A$.

In the continuum limit, when the lattice spacing tends to zero, the positional changes of the atoms can be described by a displacement field $\mathbf{u}(\mathbf{x})$. To linear approximation we define the symmetric tensor called strain as

$$u_{ij}(\mathbf{x}) = \frac{1}{2}[\partial_i u_j(\mathbf{x}) + \partial_j u_i(\mathbf{x})]. \tag{2}$$

In terms of strain the stress has the form

$$\sigma_{ij} = C_{ijkl} u_{kl}, \tag{3}$$

where for isotropic crystals

$$C_{ijkl} = \mu(\delta_{ik}\delta_{jl} + \delta_{il}\delta_{jk}) + \frac{2\mu\nu}{1-(d-1)\nu}\delta_{ij}\delta_{kl}, \tag{4}$$

$\mu$ being the shear modulus, $\nu$ the Poisson number, and $d$ the embedding dimension of the crystal.

We can introduce a gauge field $\chi(\mathbf{x})$, known in the literature as the Airy stress function, which has the property that its double curl is equal to the stress tensor,[40]

$$\sigma_{ij}(\mathbf{x}) = \varepsilon_{ikl}\varepsilon_{jmn}\partial_k\partial_m\chi_{ln}(\mathbf{x}). \tag{5}$$

This representation has the advantage of being automatically symmetric if $\chi_{ln}$ is.

The total defect density $\eta(\mathbf{x})$ is defined as the double curl of the strain tensor,[40]

$$\eta_{ij}(\mathbf{x}) = \varepsilon_{ikl}\varepsilon_{jmn}\partial_k\partial_m u_{ln}(\mathbf{x}). \tag{6}$$

In analogy with the current density of magnetism, we can introduce the density for dislocations as

$$\alpha_{ij}(\mathbf{x}) = \varepsilon_{ikl}\partial_k\partial_l u_j(\mathbf{x}). \tag{7}$$

The defect density can be expressed as a function of the dislocation density tensor as

$$\eta_{ij} = \frac{1}{2}(\varepsilon_{ikl}\partial_k\alpha_{jl} + \varepsilon_{jkl}\partial_k\alpha_{il}). \tag{8}$$

The knowledge of the total defect density makes it possible to calculate the stress function $\chi$ from the field equation[42]

$$\nabla^4\chi_{ij} = c_d\eta_{ij}, \tag{9}$$

where $c_d \equiv 2\mu(1+\nu)$ for real 2D crystals, such as, e.g., the Abrikosov vortex lattice in thin film superconductors, and $c_d \equiv 2\mu/(1-\nu)$ for 3D crystals.

For a straight edge dislocation with unit line vector $\boldsymbol{l}$ positioned at $\mathbf{x}_0$, the dislocation density tensor components are given by

$$\alpha_{ij}(\mathbf{x}) = l_i b_j \delta(\mathbf{x}-\mathbf{x}_0). \tag{10}$$

In two dimensions, for which the defect line degenerates into a point, the density tensor of dislocation reduces to

$$\alpha_i(\mathbf{x}) \equiv \alpha_{3i}(\mathbf{x}) = \varepsilon_{kl}\partial_k\partial_l u_i(\mathbf{x}) = b_i\delta(\mathbf{x}-\mathbf{x}_0). \tag{11}$$

With these notations, from Eq. (9) for the quasi-2D crystal we have ($\chi \equiv \chi_{33}$)

$$\nabla^4\chi = \frac{2\mu}{1-\nu}(\partial_1\alpha_{32} - \partial_2\alpha_{31}). \tag{12}$$

The stress components can be expressed as a function of the field $\chi$ as [see Eq. (5)]

$$\sigma_{11} = \partial_2^2\chi, \quad \sigma_{22} = \partial_1^2\chi, \quad \text{and} \quad \sigma_{12} = -\partial_1\partial_2\chi. \tag{13}$$

### B. Coarse-grained dynamics

It is widely accepted that, if the crystal has a large Peierls barrier, the inertial forces arising from the dislocation's acceleration are negligible compared to the drag forces, which are taken to be proportional to the dislocation velocity. Then the glide and climb velocity of the $i$th dislocation can be given by

$$\mathbf{v}_g^i = \Gamma_g \frac{\mathbf{F}^i\mathbf{b}^i}{b}\frac{\mathbf{b}^i}{b} \quad \text{and} \quad \mathbf{v}_c^i = \Gamma_c(\mathbf{F}^i\mathbf{n}^i)\mathbf{n}^i, \tag{14}$$

where the Peach-Koehler force $\mathbf{F}$ is given by Eq. (1), $\mathbf{n} = \boldsymbol{l}\times\mathbf{b}/b$ is a unit vector perpendicular to the Burgers vector $\mathbf{b}$, and $\Gamma_{g,c}$ represent the temperature-dependent glide and climb damping factors of the dislocation.

To predict the macroscopic response of the dislocation system, we should try to operate with locally averaged quantities, like the dislocation density tensor, stress, etc. The dislocation density tensor introduced by Eq. (7) is a highly singular quantity. More precisely, it is proportional to $\delta$ functions along the dislocation lines. During the evolution of the dislocation system these $\delta$ functions do not "spread out." Averaging the dislocation density tensor locally is equivalent to convolving it with a window function. In the literature this procedure is called homogenization or coarse graining. The coarse-graining procedure is not sensitive to the actual window function shape and its width. For any window function $w(\mathbf{r})$ we define the coarse-grained quantity $X$ as

$$\langle X(\mathbf{r})\rangle = \int w(\mathbf{r}-\mathbf{r}')X(\mathbf{r}')d\mathbf{r}'. \tag{15}$$

It is easy to show that the coarse-grained fields are related to each other in the same way as the discrete ones:

$$\nabla^4\langle\chi\rangle = \frac{2\mu}{1-\nu}[\partial_1\langle\alpha_{32}\rangle - \partial_2\langle\alpha_{31}\rangle], \tag{16}$$

$$\langle\sigma_{ij}\rangle = \varepsilon_{ik}\varepsilon_{jm}\partial_k\partial_m\langle\chi\rangle. \tag{17}$$

The above results make it possible to set up a mesoscale simulation method. Let us consider $N$ parallel edge dislocations in an $L\times L$ size square simulation area divided into cells with an appropriate coarse-grain size. The dynamics of the system is defined by repeating the following steps: First, the smoothed-out dislocation density tensor components $\alpha_{32}$ and $\alpha_{31}$ are determined by counting the dislocations in each cell. After this, the coarse-grained stress tensor components are determined from Eqs. (16) and (17) (this is done efficiently using the convolution theorem of Fourier analysis) for each cell. Finally, each dislocation is moved under the action of the local stress according to Eqs. (1) and (14). By considering $M$ mesh points in both the $x_1$ and $x_2$ directions, the first-order discretized operators in the Fourier space corresponding to $\partial_1$, $\partial_2$, $\partial_1^2$, and $\partial_2^2$ can be given as[37,41]

$$D_m = i\frac{M}{L}\sin\left(\frac{2\pi}{M}m\right), \tag{18}$$

$$D_m^2 = 2\frac{M^2}{L^2}\left[\cos\left(\frac{2\pi}{M}m\right) - 1\right], \tag{19}$$

where $m=\overline{0,M-1}$ denotes the indices of the mesh points in the $x_1$ and $x_2$ directions. Then Eqs. (17) read[37,41]

$$\tilde{\sigma}_{11}(l,m) = c_d D_l D_l \frac{b_2 D_l - b_1 D_m}{[D_l^2 + D_m^2]^2},$$

$$\tilde{\sigma}_{22}(l,m) = c_d D_m D_m \frac{b_2 D_l - b_1 D_m}{[D_l^2 + D_m^2]^2},$$

$$\tilde{\sigma}_{12}(l,m) = c_d D_l D_m \frac{b_1 D_m - b_2 D_l}{[D_l^2 + D_m^2]^2}. \tag{20}$$

The inverse discrete Fourier transforms of the above expressions give the corresponding stress components at the grid points. Certainly, if two dislocations are closer to each other than the grid distance the approximate stresses obtained by the method explained above cannot be applied to calculate the interaction force between the two dislocations. In order to solve this problem inside the box the stress expressions corresponding to an infinite body can be used[42]

$$\sigma_{11}^{\text{ind}} = \frac{c_d}{4\pi}\frac{b_2 x_1(x_1^2 - x_2^2) - b_1 x_2(3x_1^2 + x_2^2)}{(x_1^2 + x_2^2)^2}, \tag{21}$$

$$\sigma_{22}^{\text{ind}} = \frac{c_d}{4\pi}\frac{b_1 x_2(x_1^2 - x_2^2) + b_2 x_1(x_1^2 + 3x_2^2)}{(x_1^2 + x_2^2)^2}, \tag{22}$$

$$\sigma_{12}^{\text{ind}} = \frac{c_d}{4\pi}\frac{(x_1^2 - x_2^2)(b_1 x_1 + b_2 x_2)}{(x_1^2 + x_2^2)^2}. \tag{23}$$

Therefore the total stress acting on the $i$th dislocation being in the box indexed by $(l,m)$ is

$$\hat{\sigma}(\mathbf{r}_i) = \hat{\sigma}^{sf}(l,m) + \sum_j \hat{\sigma}^{\text{ind}}(\mathbf{r}_i - \mathbf{r}_j), \tag{24}$$

in which the sum needs to be performed only for those dislocations that are in the same box as the $i$th dislocation, and $\hat{\sigma}^{sf}(l,m)$ is the Fourier transform of

$$\tilde{\sigma}_{11}^{sf}(l,m) = c_d D_l D_l \frac{\tilde{\alpha}_2(l,m)D_l - \tilde{\alpha}_1(l,m)D_m}{[D_l^2 + D_m^2]^2},$$

$$\tilde{\sigma}_{22}^{sf}(l,m) = c_d D_m D_m \frac{\tilde{\alpha}_2(l,m)D_l - \tilde{\alpha}_1(l,m)D_m}{[D_l^2 + D_m^2]^2},$$

$$\tilde{\sigma}_{12}^{sf}(l,m) = c_d D_l D_m \frac{\tilde{\alpha}_1(l,m)D_m - \tilde{\alpha}_2(l,m)D_l}{[D_l^2 + D_m^2]^2}, \tag{25}$$

where $\tilde{\alpha}_i(l,m)$ is the Fourier transform of the coarse-grained dislocation Burgers vector field $\alpha_i(l,m)$.

### C. The model

Stresses arising during the normal operation of the components operating at high temperatures under extreme loading conditions have multiple components and can activate many slip systems at the same time. For simulations we have chosen a three-slip system, because the results can be directly applied to the Abrikosov lattice formed by the vortices in type-II superconductors too. Our simplified model consist of $N$ straight, parallel edge dislocations with line direction (0, 0, 1) and Burgers vectors defined by the directions $\pm(\cos(m\pi/3),\sin(m\pi/3),0)$, $m=1,2,3$. This system is effectively 2D, representing a cross section of the 3D crystal, and is equivalent to the slip geometry of the triangular lattice structure formed by the vortices in type-II superconductors. Periodic boundary conditions are assumed, which means that the square box of size $L\times L$ is replicated in each supercell. Lattice rotations are ignored.

The dislocations are initially randomly distributed in the supercell and are assumed to be presented in an equal number in each slip system so that the net Burgers vector is null. To avoid starting our simulations from these unphysical configurations, we first relax the system until it reaches a metastable configuration. During this relaxation the number of dislocations is reduced due to dislocation annihilation. In our model we annihilate a dislocation dipole when the distance between the individual dislocations with opposite Burgers vectors is shorter than a preassigned annihilation distance (when a pair of them on the same glide axis but of opposite signs came closer to each other than the grid distance $L/M$ they were taken out of the system). To keep our model as simple as possible, dislocation multiplication due to forest dislocations is ignored.

The outlined simulation method is applied to the relaxed dislocation configuration described above. We assume an overdamped dynamics in which the dislocation climb and glide velocities proportional to the total force perpendicular

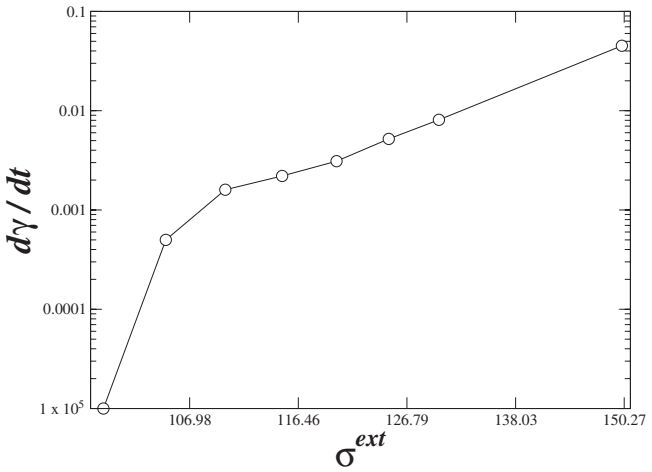


FIG. 1. Steady-state value of the strain rate (averaged over 30 independent configurations) as a function of the applied stress in dimensionless units set by Eqs. (26).

and parallel to the Burgers vector of the dislocations are given by Eq. (14). The coarse-grained quantities are determined by dividing the main supercell in $256 \times 256$ boxes. The Peach-Koehler force acting on the $i$th dislocation is calculated from Eq. (1), where the total stress acting on the $i$th dislocation is considered the sum of the coarse-grained stress (24) calculated at each time step with a fast Fourier transformation method (the above method can be considered as a special fast multipole expansion method), the external stress and the Peierls stress. To integrate numerically the $N$ coupled equations of motion (14) an adaptive step size fifth-order Runge-Kutta algorithm is used.

To eliminate material parameters, without restricting the generality, we set $c_d=1$ and the dimensionless variables

$$\mathbf{r} \to \mathbf{r}/L, \quad t \to t\Gamma_g c_d b^2/4\pi L^2 \tag{26}$$

are introduced. The arbitrary value $10^{-4}c_d$ was chosen for the Peierls stress, considered constant in space.

## III. RESULTS

To study the influence of climb on dislocation pattern formation in multislip systems an initially random dislocation distribution in three-slip configuration was relaxed at low temperature (without climb and externally applied stress) until it reached a metastable configuration. Using the metastable configuration as initial configuration, two simulations—one without climb $\Gamma_c/\Gamma_g=0$ and one with climb $\Gamma_c/\Gamma_g=0.001$—were performed, by fatiguing the sample with a sinusoidal external stress applied parallel to the $x_1$ direction. The amplitude of the external stress was chosen to be much larger than the critical resolved shear stress of the sample. To determine the critical stress, we analyzed the relaxation of 30 independent, initially random dislocation configurations. After the relaxation to a metastable state, a constant external shear stress was applied. For stresses lower than a critical value the plastic strain rate, defined as

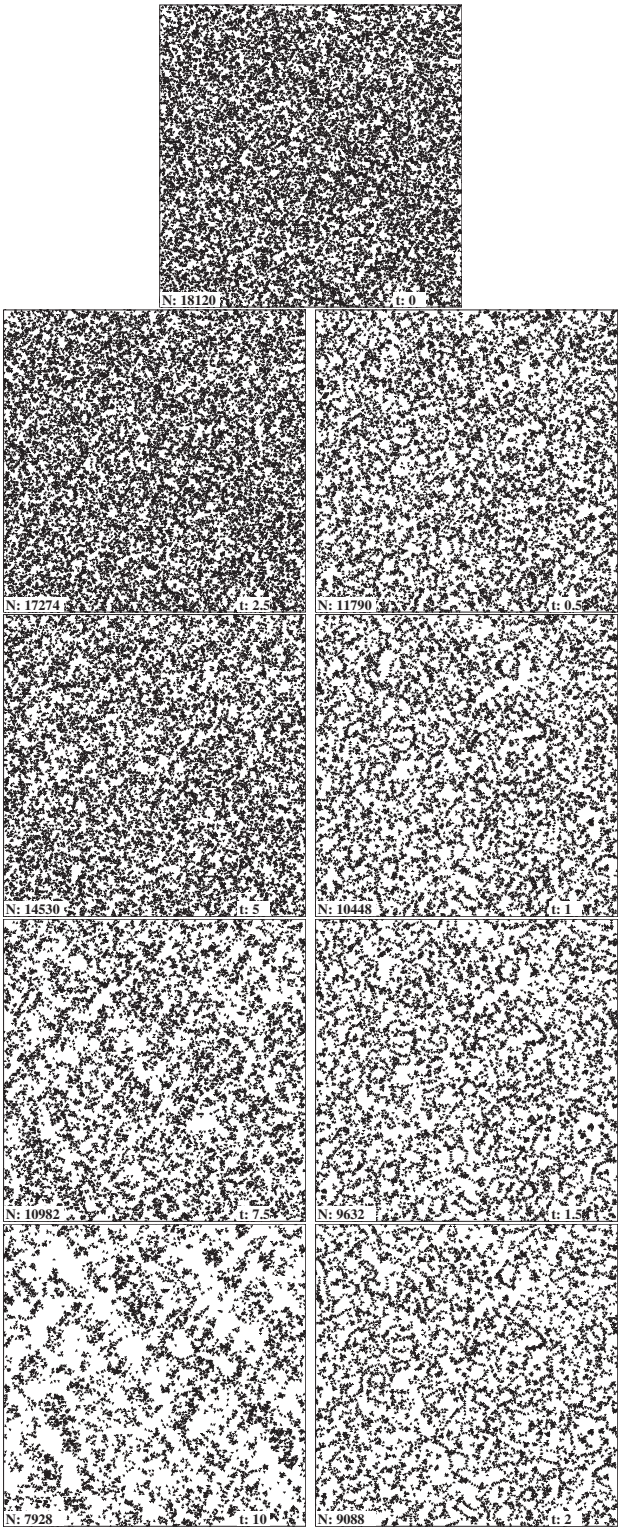


FIG. 2. Time evolution of dislocation patterns in absence of climb (left) and with climb (right). The number of dislocations is shown in the bottom left corner, while the elapsed time in units of the period of external stress is shown in the bottom right corners.

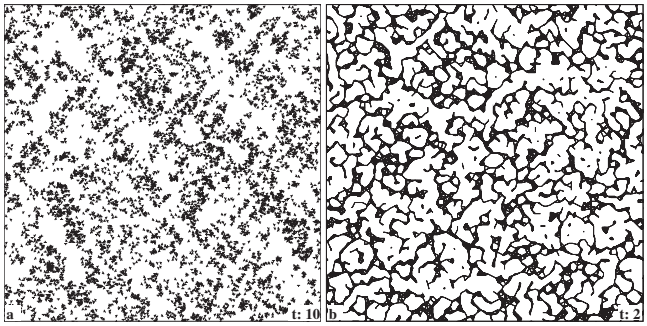


FIG. 3. Fractal (a) and cell (b) structures (from Fig. 2) developed during fatigue in the absence (a) and presence (b) of climb. The cells are identified by a technique described in Ref. 37; the lines represent dislocation walls.

$$\frac{d\gamma}{dt} = \frac{1}{b}\sum_{i=1}^{N} [(\mathbf{b}^i\mathbf{v}^i)(\mathbf{n}^i \circ \mathbf{b}^i) - (\mathbf{n}^i\mathbf{v}^i)(\mathbf{b}^i \circ \mathbf{b}^i)]\delta(\mathbf{r} - \mathbf{r}^i)$$

$$= \sum_{i=1}^{N} \begin{vmatrix} -b_1^i v_2^i & -b_2^i v_2^i \\ b_1^i v_1^i & b_2^i v_1^i \end{vmatrix}, \tag{27}$$

decays exponentially to zero (here the operator $\circ$ represents the dyadic product). For high stresses the strain rate reaches a plateau indicating a linear regime. Figure 1 shows the steady state strain rate calculated by averaging over the 30 different random configurations as a function of stress.

To see the effect of climb on pattern formation during fatigue we started two simulations from the relaxed metastable state, applying a sinusoidal external stress with an amplitude corresponding to the linear regime. In our dimensionless units given by Eq. (26) we have chosen a resolved shear stress parallel to the $x_1$ direction $\sigma^{\text{ext}}(t) = 150 \sin(0.2\pi t)$. The time evolution of the system with and without climb (corresponding to high and low temperatures) is shown in Fig. 2. When climb is enabled, formation of cells is observed (right snapshots). In the absence of climb (left snapshots) the morphology of the dislocation pattern is significantly different from the case when climb is present.

The two different type of patterns were analyzed to estimate their fractal dimension by the box-counting method. In the box-counting method for grids of square boxes with edge length $l$, the number $N(l)$ of boxes containing at least one dislocation is determined. The relation $N(l) \sim l^{-D_B}$ defines the "box-counting" dimension $D_B$.

To better visualize the cells, we apply a geometrical definition of a cell in the simulations with climb (the procedure is described in detail in Ref. 37) as follows. For a given dislocation configuration we perform Delaunay triangulation.

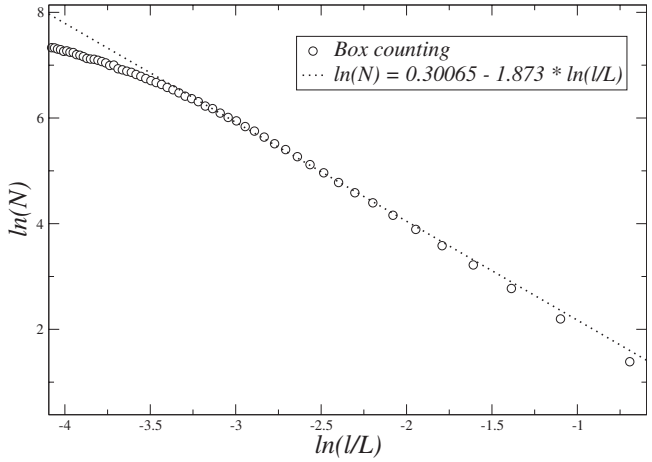


FIG. 4. Box-counting analysis of the cell structure in Fig. 2 developed in the absence of climb during ten cycles of the external stress.

Then removing (clipping) all links longer than a certain value $d_{\max}$ depending on the dislocation density yields a graph wherein the contiguous areas enclosed by loops are identified as cells [Fig. 3(b)]. For the cell-like dislocation patterns investigated, the box-counting method gives a trivial box-counting dimension 2.

Without climb the emerged cell structure shows self-similarity properties on limited length scales. The relatively low number of dislocations in this case does not permit a precise determination of the box-counting dimension. Figure 4 displays the results of the box-counting analysis on the dislocation pattern obtained after ten cycles in absence of climb. The value of $D_B \approx 1.87$ confirms reports by others.[31,36]

In conclusion, the analysis reported in the present work evidences that the dislocation cell structures formed during plastic deformation of fcc single crystals oriented for multiple slip show scaling behavior in the absence of climb. When climb is activated by temperature or other factors, the self-similarity of the developed cell structure breaks down for otherwise similar deformation conditions and a transition from fractal patterns to more homogeneous dislocation structures, characterized in terms of an average cell size, takes place.

## ACKNOWLEDGMENTS

This work was performed within the framework of the Swiss Generation IV project. Computational time on the IBM-SYSTEM P5 cluster at the Swiss National Supercomputing Center is gratefully acknowledged.

*Botond.Bako@psi.ch

[1] Generation IV Technology Roadmap, http://gif.inel.gov/roadmap/
[2] P. J. Jackson, Prog. Mater. Sci. **29**, 139 (1984).
[3] H. Mughrabi, T. Ungar, W. Kienle, and M. Wilkens, Philos. Mag. A **53**, 793 (1986).
[4] D. S. Fisher, B. I. Halperin, and R. Morf, Phys. Rev. B **20**, 4692 (1979).
[5] G. Blatter *et al.*, Rev. Mod. Phys. **66**, 1125 (1994).

[6] R. Seshadri and R. M. Westervelt, Phys. Rev. B **46**, 5142 (1992).
[7] G. Grüner, Rev. Mod. Phys. **60**, 1129 (1988).
[8] C. A. Murray and D. H. V. Winkle, Phys. Rev. Lett. **58**, 1200 (1987).
[9] R. A. Quinn and J. Goree, Phys. Rev. E **64**, 051404 (2001).
[10] K. Moon, R. T. Scalettar, and G. T. Zimanyi, Phys. Rev. Lett. **77**, 2778 (1996).
[11] B. I. Halperin and D. R. Nelson, Phys. Rev. Lett. **41**, 121 (1978).
[12] L. Kubin, in *Material Science and Technology: A Comprehensive Treatment*, edited by R. W. Chan, P. Haasen, and E. J. Kramer (VHC, Weinheim, 1993), Vol. 6.
[13] L. Kubin, in *Stability of Materials*, edited by A. Gonis, P. Turchi, and J. Kudrnovsky, NATO Advanced Studies Institute on Stability of Materials (Plenum, New York, 1996), Vol. 355, p. 99.
[14] D. Kuhlmann-Wilsdorf and J. H. van der Merve, Mater. Sci. Eng. **55**, 79 (1982).
[15] D. L. Holt, J. Appl. Phys. **41**, 3179 (1970).
[16] J. M. Rickman and J. Vinals, Philos. Mag. A **75**, 1251 (1997).
[17] D. Walgraef and E. C. Aifantis, J. Appl. Phys. **15**, 688 (1985).
[18] E. C. Aifantis, Mater. Sci. Eng. **81**, 563 (1986).
[19] C. Schiller and D. Walgraef, Acta Metall. Mater. **36**, 563 (1988).
[20] J. Kratochvil and S. Libovicky, Scr. Metall. **20**, 1625 (1986).
[21] J. Kratochvil, Mater. Sci. Eng., A **164**, 15 (1993).
[22] A. Franek, R. Kalus, and J. Kratochvil, Philos. Mag. A **64**, 497 (1991).
[23] P. Hähner, Acta Mater. **44**, 2345 (1996).
[24] P. Hähner, Appl. Phys. A: Mater. Sci. Process. **62**, 473 (1996).
[25] A. Gullouglu, D. Srolovitz, R. LeSar, and P. Lomdahl, Scr. Metall. **23**, 1347 (1989).
[26] A. N. Gullouglu and C. S. Hartley, Modell. Simul. Mater. Sci. Eng. **1**, 1 (1992).
[27] A. N. Gullouglu and C. S. Hartley, Modell. Simul. Mater. Sci. Eng. **1**, 383 (1992).
[28] R. J. Amodeo and N. M. Ghoniem, Phys. Rev. B **41**, 6958 (1989).
[29] V. A. Lubarda, J. A. Blume, and A. Needleman, Acta Metall. Mater. **41**, 625 (1993).
[30] H. H. M. Cleveringa, E. Van der Giessen, and A. Needleman, Acta Mater. **45**, 3163 (1997).
[31] P. Hähner, K. Bay, and M. Zaiser, Phys. Rev. Lett. **81**, 2470 (1998).
[32] P. Hähner and M. Zaiser, Mater. Sci. Eng., A **272**, 443 (1999).
[33] P. Hähner, Scr. Mater. **47**, 705 (2002).
[34] R. Thomson, M. Koslowski, and R. LeSar, Phys. Rev. B **73**, 024104 (2006).
[35] B. Bakó and I. Groma, Phys. Rev. B **60**, 122 (1999).
[36] I. Groma and B. Bakó, Phys. Rev. Lett. **84**, 1487 (2000).
[37] B. Bakó, I. Groma, G. Györgyi, and G. Zimányi, Comput. Mater. Sci. **38**, 22 (2006).
[38] R. Madec, B. Devincre, and L. P. Kubin, Scr. Mater. **47**, 689 (2002).
[39] N. Hansen and D. Kuhlmann-Wilsdorf, Mater. Sci. Eng. **81**, 141 (1986).
[40] H. Kleinert, *Gauge Fields in Condensed Matter* (World Scientific, Singapore, 1989), Vol. II.
[41] B. Bakó, I. Groma, G. Györgyi, and G. T. Zimányi, Phys. Rev. Lett. **98**, 075701 (2007).
[42] E. Kröner, *Physics of Defects*, edited by R. Balian *et al.*, Proceedings of the Les Houches Summer School of Theoretical Physics, XXXV, 1980 (North-Holland, Amsterdam, 1981).